

Response to the Referees of the manuscript:

“Structure of the upper mantle in the north-western and central United States from USArray S-receiver functions” by R. Kind et al.

Responses in red

See bottom for revised manuscript with significant changes marked

B. Romanowicz

General comments

This paper presents a comprehensive - and impressive - analysis of S receiver function data over the continental US, with dense sampling owing to the availability of data from USArray. The paper is well written and the presented cross-sections show some interesting features, adding to the existing evidence for complexity of lithospheric structure contrasted across the boundary between the western tectonically active part of the US and the central craton. It also offers additional support for the presence of a thin low velocity zone atop the 400 km discontinuity.

My primary comments concern the intriguing interpretation given by the authors (Fig. 10) and described in detail in section 4 of the paper. I am somewhat skeptical about the lines drawn on figures 8 and 9, and meant to describe dipping structures. It is quite clear that the authors document the rather abrupt termination of the ~100 km depth western US LAB somewhere between the Sevier Thrust Belt and the Rocky Mountain Front, and that the structure changes very significantly going into the craton. However, I find the dipping broken lines drawn in figures 8 and 9 reflecting more a point of view of the authors rather than a hard fact. So, it would be important to also show these cross-sections without the interpretation lines. **We have added two new figures which make our correlations more clear (new figures 10 and 11, Fig.11 without marks). Of course, there could be debates about some of the correlations. However, we think there is no doubt about the existence of west dipping structures in the mantle lithosphere at the margin of the craton.** Indeed, what *I see*, particularly at latitudes below 43° (sections g->n in figure 8) but also looking across the N-S sections in Figure 9e-g, is that east of about 110°W longitude, there is a thick zone of almost continuous "negative" reflectors (blue colors) in the depth range 100 to 200 km, with no obvious justification for drawing tilted lines across them. This zone is particularly reflective and strong in sections 9b and 9e, which are singled out by the authors for their cartoon shown in Fig. 10. However, it is also present in other sections, although less clearly, indicating significant lateral variability of the reflectors.

In fact, this thick zone of negative reflectors corresponds well with what was already documented, a long time ago, from long range profile experiments, as a zone of strong scattering (e.g. Thybo and Perchuc, 200x). It also agrees with the zone of somewhat reduced velocity found in some tomographic models under all cratons (e.g. Lekic and Romanowicz, 2011). In other words, it fits well with the idea of a layered cratonic lithosphere, with an MLD marking the top of a complex zone of varying thickness and, on average, somewhat reduced shear velocities, and an LAB within the craton that is around 200 km depth, and with less topography, as found from waveform anisotropic tomography (Yuan and Romanowicz, 2010; Yuan et al., 2011).

There are many MLD observations in the cratonic US. We are not saying that this is a new observation in our paper. The new point is the structure of MLD and LAB at the margin of the craton, which was much less resolved so far. We have added references to earlier observations of scattering in the lower lithosphere in long range controlled source profiles.

I can just as well draw a vertical line at about -112-113°W in panels i,j,k,l of Figure 8 marking the sharp transition between the thick cratonic lithosphere to the East and the thinner western US one to the west, consistent with tomography (e.g figure 11ab in Yuan et al., 2011), and, for example, the observation of SP phases horizontally deflected along the Rocky Mountain Front (e.g. Zheng and Romanowicz, 2012).

Earlier papers on the cratonic margin are seeing a more or less gradual thickening of the lithosphere from west to east. We have added the references you are mentioning. We are also seeing a similar step like change at about -102°W, however only on an EW profile along 33-38°N (see the new Fig.10). In other EW profiles

the observed steps are related to west or east inclined discontinuities between about -102 to -112°W (see especially the new Figs.10 and 11). An exception seems to be the more complicated profile along 43-46°N (see the new Figs.10 and 11). These new figures add more details to the same observations in the migrated data of the Figs.8 and 9 and make more clear the west dipping structures between about 39 and 45°N.

This layering and its abrupt change across the RMF is also clearly visible in azimuthal anisotropy (e.g. Yuan and Romanowicz, 2010). Here the authors mention that they find no evidence for azimuthal anisotropy from receiver functions. There is actually evidence for azimuthal anisotropy layering in the craton from many regional studies of SKS splitting (e.g. Deschamps et al., 2008) or surface wave analysis (e.g. Derbyshire et al., 2013) and most recently, from an analysis combining surface wave dispersion, SKS splitting and receiver functions (Leiva et al., AGU abstract, 2014; Bodin et al., *in preparation*), yielding results that are in good agreement with anisotropic waveform tomography beneath a sample of stations on the craton. The fact that the authors do not find evidence for anisotropy in their receiver functions may be due to 1) a faint signal in the receiver functions coupled with insufficient azimuthal coverage at most stations that have not been recording for long enough times; 2) the use of a reference 1D model for the migration to depth.

We are not questioning such anisotropy observations. It is not clear why S receiver functions do not see such anisotropy effects. It is probably not the azimuthal source distribution which is relatively good (see Fig.2). The signal-to-noise ratio is also very good. We did not apply migration, we stayed in time domain in Fig.5 and applied the 1D model for distance move-out correction. Other models would change move-out corrections by only a few percent.

How the MLD defined by the long wavelength azimuthal anisotropy study (Yuan and Romanowicz, 2010) relates in detail to the observed onset of scattering in the receiver functions remains to be determined.

We like to point out that MLD and LAB appear only in relatively long period filtered data as single discontinuities. In unfiltered data they dissolve in several scattered small scale discontinuities. This is different, for example, for the Moho or 410 discontinuity which get sharper when shorter period data are used.

Further comments:

On page 5, line 23-27, the authors briefly mention that one can analyze converted phases without deconvolution, but they make an intriguing statement: "However, the advantages of deconvolution in improving the signal to noise ratio prevail". It would be nice if the authors would expand and provide supportive argumentation to this statement. Indeed, one can also stack records without deconvolution, leading to superior signal to noise ratio. One can discuss the advantages and disadvantages of deconvolution versus direct convolution using synthetic seismograms (e.g. Bodin et al., 2014) at length, but brushing aside the latter approach as inferior without justification is not very satisfying.

We have changed that statement

In figure 1, the authors show a map of earthquake coverage for their study. I think this is a bit misleading: most likely no one station (except for some long term permanent stations) sees such a good azimuthal coverage. It would be more informative to show several panels, corresponding each to a particular time period of the deployment of USArray.

We have now explained in more detail the recording conditions of USARRAY.

Technical Details

On page 8, line 3 - typo: "discontinuity IS given"

In figure 9 caption: please explain the abbreviations: ST, RMF, MCRG.

done

References

- Bodin, T., H. Yuan and B. Romanowicz (2014) Inversion of receiver functions without deconvolution - application to the Indian craton, *Geophys. J. Int.*, 196, 1025- 1033.
- Darbyshire, Fiona A., Eaton, David W., and Bastow, Ian D. (2013), Seismic imaging of the lithosphere beneath Hudson Bay: Episodic growth of the Laurentian mantle keel, *Earth Planet. Sci. Lett.*, 373(0), 179-193, doi:http://dx.doi.org/10.1016/j.epsl.2013.05.002.
- Deschamps, F., S. Lebedev, T. Meier, and J. Trampert (2008a), Stratified seismic anisotropy reveals past and present deformation beneath the East-central United States, *Earth Planet. Sci. Lett.*, 274(3-4), 489-498.
- Leiva, J., T. Bodin and B. Romanowicz (2014) Towards an Improved Joint Inversion of Receiver Functions, SKS Splitting, and Surface Wave Dispersion Data for Layering in the North American Craton, Fall 2014 AGU, Abstract.
- Lekic, V. and B. Romanowicz (2011) Tectonic regionalization without a priori information: a cluster analysis of upper mantle tomography, *Earth Planet. Sci. Lett.*, 308, 151-160.
- Thybo, H. and E. Perchuc (200x) *Science*
- Yuan, H. and B. Romanowicz (2010) Lithospheric Layering in the North American Continent, *Nature*. 466, 1063-1069.
- Yuan, H. B. Romanowicz, K. Fischer and D. Abt (2011) 3-D shear wave radially and azimuthally anisotropic velocity model of the north American upper mantle, *Geophys. J. Int.*, 184, 1237-1260, doi:10.1111/j.1365-246X.2010.04901.x
- Zheng Z. and B. Romanowicz (2012) "Do double "SS precursors" mean double discontinuities *Geophys. J. Int.*, 191, 1361-1373.

Anonymous Referee #2

While much of the U.S. has been examined before using S receiver functions, it is important that multiple studies are performed using similar techniques on similar datasets to insure reproducibility of results and to identify points of contrast, which in turn offers a rough method of understanding uncertainty.

I am not a practitioner of the receiver function methodology, although I understand the basics and know the authors as having a track record of high-quality work. With that in mind, the analysis of the data looks reasonable, and I appreciate the careful attention paid to identifying the nature of the conversion identified as the MLD or LAB (like in Figure 3).

However, there is no interpretation of the physical cause of the various impedance contrasts identified, and without this interpretation, the study lacks importance. Discontinuities are identified as the MLD or LAB by default (as the authors state in the introduction). However, the study would be more interesting if the some constraints were put on the impedance contrast, and thus physical characteristics, of the features producing the S-P conversions. One could also envision examining the layers in the context of the pressure and temperature at which they occur and then considering what causes are plausible.

It was not really the goal of the present paper to discuss in general the 1D structure of the MLD and LAB. However we have added more comments to this point. The main goal is to determine the topography of these discontinuities especially in collision zones. For example we found that the MLD might move gradually due to collision from 100 km depth to 200 km depth. Such a possibility is not explained so far in any model of the MLD. Also the MLD and LAB are not usual discontinuities like Moho or 410 discontinuity, which get sharper when shorter period seismic waves are used. MLD and LAB appear only as a single discontinuity if relatively long period data are used. They dissolve in many scattered discontinuities when no filter is used. This point is not generally known and it requires more observational studies before modeling can be successful.

Partially because there is no attempt to examine the cause of the imaged structures I also found the conclusion rather unsatisfying: complicated structures are interpreted as being caused by the collision of the Farallon and Laurentia plates. What exactly does this mean? Please give more specifics.

We have discussed this point in more detail and described where which discontinuity of which plate is deforming in which way. It is to our knowledge a new discovery that western dipping structures exist in the mantle lithosphere in the collision region of the Farallon and Laurentia plates. This collision zone is extremely complicated and the lithosphere is not just thickening from west to east.

Also, I'm not sure I follow the reasoning that suggests the lack of a low velocity layer just above the 410 km discontinuity as being consistent with cratonic tectosphere. Under the transition zone water filter hypothesis, doesn't a low velocity layer indicate melt produced when hydrated mantle moves upward through the 410 discontinuity; hence, I would think the lack of a low velocity layer would just mean no vertical movement. But perhaps I am a little confused here.

This is a difficult question. We have reduced this statement since such observations are still rare.

All in all, this paper reads like a study that is not quite complete.

We have tried to make it more interesting for the non-seismological reader. However the main point is observation of the west dipping structures in the mantle lithosphere in the central part of the western US and the complicated interfingering of both lithospheres. This is a highly controversial point and needs certainly confirmation. We also think that the question of the sharpness of the MLD and LAB has to be reconsidered in the light of the new S receiver function results. Our paper does not offer a final solution, we think it opens a number of new questions.

Structure of the upper mantle in the north-western and central United States from USArray S-receiver functions

Rainer Kind^{1,2,*}, Xiaohui Yuan¹, James Mechie¹, Forough Sodoudi¹

¹Deutsches GeoForschungsZentrum GFZ, Potsdam, Germany

²Freie Universität, Fachrichtung Geophysik, Berlin, Germany

*Corresponding author, kind@gfz-potsdam.de

Abstract

We used more than 40,000 S-receiver functions recorded by the USArray project to study the structure of the upper mantle between the Moho and the 410-km discontinuity from the Phanerozoic western United States to the cratonic central US. **In the western US we observed the lithosphere-asthenosphere boundary (LAB), and in the cratonic US we observed both, the mid-lithospheric discontinuity (MLD) and the LAB of the craton. In the northern and southern US the western LAB almost reaches the mid-continental rift system. In between these two regions the cratonic MLD is surprisingly plunging towards the west from the Rocky Mountains Front to about 200 km depth near the Sevier Thrust Belt. We interpret these complex structures of the seismic discontinuities in the mantle lithosphere as an indication of interfingering of the colliding Farallon and Laurentia plates. Unfiltered S receiver function data reveal that the LAB and MLD are not single discontinuities but consist of many small scale laminated discontinuities, which only appear as single discontinuities after longer period filtering.** We also observe the Lehmann discontinuity below the LAB and a velocity reduction about 30 km above the 410-km discontinuity.

1. Introduction

Lithospheric plates, including thick old cratons, translate over thousands of kilometers over the viscous mantle. However, relatively little is still known about the internal structure of cratons and the transition between the craton and the convecting mantle. Even after more than half a century since the general acceptance of plate tectonic theory, the lithosphere-asthenosphere boundary

(LAB) below cratons is still thought to be “elusive” (Eaton et al., 2009) and an additional velocity drop frequently observed in seismic data in the shallow cratonic lithosphere (mid-lithospheric discontinuity, or MLD) is referred to as “enigmatic” (Karato, 2012). These descriptions not only apply to the petrophysical properties of the LAB and MLD but are also a result of still inadequate seismological imaging. The lithosphere-asthenosphere system was originally a mechanical definition (Barrell, 1914) and is not a seismic definition. However, we are using the name LAB here for seismic velocity reductions observed near 200 km depth in cratons and near 100 km depth in oceans and Phanerozoic regions by tomography and receiver functions (e.g. Yuan and Romanowicz, 2010). Tomography is not directly sensitive to discontinuities and therefore the transition from lithosphere to asthenosphere is derived from the velocity-depth functions or its vertical gradients (e.g. Yoshizawa, 2014). Only a few tomography studies observed in cratons a shallow low velocity zone near 100 km depth which could be related to the MLD (e.g. Lekic and Romanowicz, 2011).

The alternative view of the deep structure of cratons, independent of the lithosphere-asthenosphere model, defines a tectosphere with the keel of the cratons reaching down to about 400 km (Jordan, 1975). This model is based on different versions of the tomography method (see Jordan and Paulson, 2013, for a summary). The tectosphere may be decoupled from the convecting mantle by a low viscosity layer directly above the 410-km discontinuity. A possibly related velocity reduction above the 410 is observed globally by Tazsin et al. (2010).

The LAB and MLD are mainly observed with receiver functions. Summaries of their global distribution are given by Rychert and Shearer (2009), Rychert et al. (2010), Fischer et al. (2010) and Kind et al. (2012). Since the MLD and in some places the cratonic LAB are relatively well observed with seismic body waves, both discontinuities must be relatively sharp. Rychert et al. (2007) deduced from P-receiver functions a sharpness of 11 km for the LAB at the east coast of the US. Li et al. (2007) obtained a sharpness of about 20 km in the western US using S-receiver functions. Rychert et al. (2007) concluded that the sharpness of the LAB excluded temperature variation as the single cause of the LAB. Karato (2012) suggested the grain-boundary sliding model as the cause of the MLD and LAB. This model predicts a strong MLD and weak LAB below cratons. According to Yuan and Romanowicz (2010) the North American craton consists of two layers with different chemistry and anisotropy, with the upper layer reaching to about 100 km depth being the Archean lithosphere. Selway et al. (2015) reviewed the mechanisms which could cause the MLD.

It would be difficult to show the existence of the MLD in Phanerozoic regions since here the LAB would also be expected at a similar depth. Therefore it is interesting to study the structure of the MLD and LAB at continental collision zones as in the western US. Abt et al. (2010) and Kumar

et al. (2012a,b) observed in almost the entire US only a shallow negative discontinuity near 100 km depth. This discontinuity varies to some extent in depth but nowhere does it reach 200 km depth. In the western US and at the east coast this signal was called the LAB while in the central cratonic US it was called the MLD by Abt et al. (2010), and the LAB by Rychert and Shearer (2009) and Kumar et al. (2012a,b). Levander and Miller (2012) have mapped the Phanerozoic LAB in the western US. More detailed regional studies in the western US are published by Rychert et al. (2005, 2007), Li et al. (2007), Hopper et al. (2014), Hansen et al. (2013), Foster et al. (2014) and Lekic and Fischer (2014). Rare observations of the cratonic LAB near about 200 km depth have been obtained by Foster et al. (2014) in the US. Similar observations in other cratons have been obtained in Canada (Miller and Eaton, 2010), Scandinavia (Kind et al., 2013) and South Africa (Sodoudi et al., 2013).

The structure of the mantle lithosphere in western North America was formed by the collision of the Farallon plate with the Laurentia craton and was first resolved by tomographic studies. The subducted Farallon plate is visible in the upper and lower mantle, even below the eastern United States (Grand, 1994; Schmandt and Lin, 2014). The collision with the Precambrian North American craton about 50 million years ago during the Laramide orogeny tore and broke the Farallon plate. An example is the “big break” in the western US of Sigloch et al. (2008) and Sigloch (2011) and references therein, or the vertical high velocity “curtain” near the longitude of Yellowstone (Schmandt and Humphreys, 2011). **The boundary of the craton follows approximately the Rocky Mountains Front (see for example Yuan et al., 2011 and Zheng and Romanowicz, 2012).**

2. Methodology

We use the S-receiver function technique (meaning S-to-P conversions) to image seismic discontinuities between the crust-mantle boundary (Moho) and the seismic discontinuity at 410 km depth (see e.g. Yuan et al., 2006 or Kind et al., 2012 for a description of the technique). The receiver function method determines the response of the Earth structure below a seismic station. Teleseismic waves arriving at a station are scattered by the underlying discontinuities, causing conversions and multiple reflections, which lead to images of the layered structure below the station.

The most important step in receiver function processing is stacking of many seismic traces in order to enhance the weakly converted waves. The simplest approach is to align many records for a given station with respect to a main phase, for example S, after amplitude and sign normalization, and sum these traces. The summation is performed for each component separately (vertical, radial and transverse). We rotated the components by theoretical backazimuth and incidence angle of the S phase and obtained approximately the P, SV and SH response of the medium below the station.

As the traveltimes moveout between the main phase and the scattered phase depends on epicentral distance, this kind of summation can, without a moveout correction, only be done in narrow epicentral distance windows (Shearer, 1991). A distance moveout correction permits summation over larger distance ranges (Yuan et al., 1997). However, a velocity model is required. Since the moveout correction can only be made for one type of phase at a time (for example P-to-S conversions, or multiples), signals traveling with different slownesses will be canceled by stacking.

Traditionally, deconvolution is used to equalize (and approximately remove) the source signals of the different earthquakes before stacking. For example, in P-receiver functions, a window around the P signal on the vertical component is used to deconvolve the radial component. We should also mention that, theoretically, deconvolution is not required in the receiver function technique. Summation of plain seismograms leads to **similar** results (see Kumar et al., 2010; Bodin et al., 2014). **Here we applied deconvolution since we obtained better signal-to-noise ratios.** Another important step in receiver function processing is the migration from the time domain into the depth domain using a known velocity model. For migration, the seismic energy is back-projected along the ray path within a given model and stacked, assuming that the energy is distributed in the Fresnel zone (Jones and Phinney, 1998; Kosarev et al., 1999; Yuan et al., 2006). The one dimensional IASP91 reference model is used for moveout correction and migration. Both moveout correction and migration are relatively insensitive to the model used.

We use S-receiver functions in the present study, which have a significant advantage over P-receiver functions for upper mantle studies. In S-receiver functions, the direct conversions arrive before the S signal while the crustal multiples arrive after the S signal. In P-receiver functions, both direct conversions and multiples arrive after the P signal. Multiples in P-receiver functions frequently overwhelm direct conversions and make it difficult to identify the true structure. However, S-receiver functions have other problems which need to be considered. In the next section we include a discussion of some problems of the interpretation of the wave field of S precursors using the example of USArray data.

3. Data

We obtained the data from the open access IRIS archive in Seattle, Washington (www.iris.edu). Most data are provided by the USArray project (www.usarray.org), which is a continent-wide temporary mobile network with a spacing of about 70 km between stations. **Stations recorded on average for about two years at one site before they were moved to another site.** The locations of the seismic stations used in this study are shown in Fig. 1. The distribution of the epicenters of the earthquakes used is shown in Fig. 2.

We have inspected manually over 200,000 records from events with magnitudes greater than 5.7 within the epicentral distance range of 60-85°. Conditions for the selection of traces were a signal-to-noise ratio of at least two in the original broadband S signal on the SV component, a good approximation of a spike by the deconvolved SV signal, low energy at the time of the spike on the P component and no obviously disturbing signals before the S arrival on the P component. This procedure appears to be robust, since several persons participated in selecting data along these lines without a visible personal influence.

Finally more than 40,000 records have been selected for our study. Next we will discuss the wave field of the S precursors of all available data in different graphical presentations. The data in most of the following figures are lowpass filtered with 8 s corner period. In Fig.3a all traces are shown as a function of the epicentral distance. The traces are summed within 0.5° windows of epicentral distance disregarding the backazimuth and station location. The same data are shown in Fig.4 as common conversion point (CCP) stacks and as a function of the station locations. Distance (or slowness) moveout corrected traces (reference slowness 6.4 s/°) are summed, with hypothetical S-to-P piercing points at 200 km depth within a certain geographical box. The back azimuth of the sources is disregarded. The boxes are aligned along west-east and south-north profiles. West-east profiles are shown in Fig.4a. The box size is 0.5° longitude and extends in the south-north direction over the entire array. South-north profiles are shown in Fig.4b. The box size is 1° latitude and extends in west-east direction also over the entire array. In Fig.5 the traces are shown from the cratonic part of the network (east of 110°W longitude) as a function of the backazimuth. There is no overlapping of windows. Neighboring stacked traces therefore do not contain any common traces.

There are obviously several seismic phases visible in Figs.3-5. Seismic phases marked red (positive) are caused by a discontinuity with downward increasing velocity. Blue phases (negative) mark downward decreasing velocity. All phases converted from the direct S phase to P are marked with black labels in Figs.3-5. These are the conversions from the Moho, two blue phases labeled LVZ1 and LVZ2, the conversion from the discontinuity at 410 km depth (marked “410”), a red discontinuity marked “Lehmann” and another blue discontinuity following closely the 410 signal and marked “LVZ410”. The Moho is not the focus of our study. The LVZ410 is observed in P- and S-receiver functions by a number of authors in different parts of the world (e.g. by Schaeffer and Bostock, 2010 in northwestern Canada; by Vinnik et al., 2010 in California and globally by Tauzin et al., 2010). It is interpreted by the presence of water causing partial melt. Jordan and Paulson (2013) discuss the role of this discontinuity for decoupling the thick continental tectosphere (which extends below the LAB) from the convecting mantle. The Lehmann discontinuity is widely

considered as the bottom of the asthenosphere. A global study of the Lehmann discontinuity is given by Gu et al. (2001).

Theoretical traveltime curves of S precursors at the above mentioned discontinuities are marked by dashed black lines in Fig.3a. They are computed using the IASP91 global reference model with three negative discontinuities (LVZ1, LVZ2 and LVZ410 at 90, 170 and 380 km depth, respectively) and one positive discontinuity (Lehmann at 270 km) added. The Moho is set at 35 km depth. LVZ1 and the 410 are clearly observed in Figs.3-5. The LVZ2 and the Lehmann discontinuity are better observed in Fig.4.

Additional seismic phases, besides the ones discussed so far are only visible in Fig.3a but not in Figs.4 and 5. Theoretical traveltime curves have been computed to explain these phases. They are marked in green. We see clear negative SKS660p and ScS660p phases from the 660 km discontinuity cutting through all other phases prior to the S arrival. These phases are strong at 68-73° and 75-79° epicentral distances and 10-30 s precursor time, and at 75-80° epicentral distance and 40-50 s precursor time, where they cut through the LVZ2 and the LVZ410 signals. However, the signals are caused by the SKS and ScS conversions at the 410 and 660 discontinuities and have very different slownesses than the S phase. This is the reason why they are canceled out in the moveout corrected and stacked signals in Figs.4 and 5. There are also surprisingly clear phases after the S signal in Fig.3a. They are the crustal multiples SPmp and SPn below the stations (see the ray path of SPn in Fig.3b), which are so far not much used to infer information about the P velocity below the stations.

There have been concerns that higher order P multiples could influence S precursors on the P component (Bock, 1994; Wilson et al., 2006). However, we do not see such phases in the complete observed precursor wave field in Fig.3a. The reason is probably that the upper mantle of the Earth is too heterogeneous to permit the efficient propagation of higher order P multiples. In Fig.6 we have computed S precursors for the one dimensional IASP91 Earth model (vertical component). We used the version of the reflectivity method by Kind (1985), which is an extension of the original method by Fuchs and Müller (1971) for different source and receiver structures. This version avoids P multiples in the theoretical seismograms, which cause a high noise level in front of the S phase making it difficult to get good S precursors. An approximated spike was used as the source time function. The strong SPn and SsPmp phases after S agree well with the data in Fig.3a. A disagreement between computed and observed seismograms is the source-side Pn in front of the S signal (Fig.6), which is not in the data (Fig.3a). This is a phase traveling as P along the surface on the source side and continuously radiating S waves downward. At the receiver side these phases are converted back to P and travel again horizontally along the surface. These phases are not observed

in the stacked S-receiver functions (Fig.3a) because of stacking of records from many regions with different structures and source depths. The same phases marked green in the data (Fig.3a) are also marked green in the theoretical seismograms in Fig.6. Note that the IASP91 model does not have an upper mantle low velocity zone, nor the Lehmann discontinuity and also not the negative discontinuity above the 410. Therefore these phases are not computed.

In order to point out another possible source of disturbing S precursors, we have computed theoretical seismograms similar to Fig.6 for different crustal models at the source and receiver sides (see Fig.7). A narrower slowness integration window was used, which excludes source-side Pn. There is a 50 km thick crust at the source side in Fig.7a and no crust is included at the source side in Fig.7b. Receiver-side crust is in both cases 40 km thick. The rotated L component is shown, which carries practically only P energy. We see ScS and SKS conversions at the 410 and 660 discontinuities, which cross the Sp conversions at the Moho and at the 410. In Fig.7c ray paths of Smp with a conversion at the receiver-side Moho (Fig.7b) and of PmSmp with an additional P-to-S conversion at the source-side Moho (Fig.7a) are shown. The PmSmp phase is visible in Fig.7a as a negative precursor of the Moho conversion, which might be mistaken in the real data as a S-to-P conversion at a negative discontinuity below the Moho underneath the station. In receiver functions, however, this phase is reduced due to summation of many events with different source depths and source-side structures. Care should be taken if single seismograms are used because it seems impossible to identify all phases uniquely in these cases.

4. Topography of the discontinuities in the mantle lithosphere

To image the topography and structure of such discontinuities in the study area we plotted in Figs.8 and 9 several depth migrated profiles and in Figs.10 and 11 several profiles in the time domain. The width of the profiles is two degrees or more of latitude or longitude. The profiles cannot be chosen much narrower because the number of traces available for summation would be too small. Each of the traces in Figs.10 and 11 was obtained by summation of several hundred traces. The depth domain profiles are chosen along great circles and the time domain data along latitude and longitude. The traces in the time domain profiles (Figs.10 and 11) are selected by the location of their S-to-P piercing points at 200 km depth. To a first approximation the precursor time may be multiplied by a factor of 10 to obtain the corresponding depth. The IASP91 model is used for depth migration in Figs.8 and 9. The first and perhaps most important task of the data interpretation is the recognition of patterns in the data. We have chosen variable width of the profiles in the different figures to show the variability of the correlations in dependence on the profile width. In the mantle lithosphere below the Moho we observe several clearly correlatable blue signals (velocity decrease

downward). We interpreted these signals as being caused by the LAB in the western US (marked with magenta lines) and the MLD in the central US (marked with yellow lines) and the cratonic LAB in the eastern US (marked with green lines). In the following we discuss the topography of each of these negative discontinuities in the mantle lithosphere.

4.1 Structure of the western LAB:

North of about 46°N the western LAB extends from the west coast to at least 100°W where it ends (Figs.8a-d and 9a). In the wider profile of Fig.9a it even seems to extend to 90°W. It is smoothly dipping from about 100 km depth at the west coast to about 200 km depth at its eastern end. Between 46-48°N the depth domain Fig.8c is not in very good agreement with the time domain Fig.10B. The reason could be that Fig.8c has more traces in the north because it follows the great circle. The western LAB is laterally very heterogeneous just north of about 45°N (see Figs.10B, C). South of about 45°N the western LAB reaches from about 114°W to about 104°W with increasing easterly extension towards the south. There is some indication of a local easterly dip also in this part of the western LAB (see Fig.8l).

North of about 46°N we have in addition indications of another negative discontinuity closer to the west coast (marked black in Fig.10). It dips steeply down to about 200 km depth before turning horizontal at this depth. We interpret this structure as the LAB of the Juan de Fuca plate without going into more detail here.

4.2 The structure of the MLD:

The MLD is marked yellow in the figures and it is visible in most profiles in the central US near 100 km depth where it is expected. It is poorly seen south of about 37°N which is probably due to insufficient data (Fig.8m-p). Between 39 and 45°N (from the northern end of the Colorado Plateau to Yellowstone) the MLD seems to dip from its normal depth near 100 km east of 100°W to about 200 km depth at about 112°W (see Figs.8 e-k and 9b) at the Sevier Thrust Belt. We note that there is in the area of 40-45°N and 112-106°W no discontinuity near 100 km depth which could be an extension of the western LAB or MLD (see Figs.9b and e). The westerly dip of the MLD is clearer in Fig.10D. There are similar indications in the profile in Fig.10E. In Fig.10C it may also be visible, although in this profile there is additionally an indication of the east dipping western LAB. This apparent crossing of discontinuities could be caused by lateral variations within the 3° latitude wide profile. The observation of such a west dipping structure in the mantle lithosphere in this part of the US seems to be new to our knowledge. We will return to this question below when Fig.11 will be discussed.

4.3 The structure of the cratonic LAB

The signals we interpreted as cratonic LAB near 200 km depth are marked green in Fig.8, 9 and 10. These signals are relatively weak in some of the narrow profiles in Fig.8. In the wider profiles in Fig.9c, f and g, the cratonic LAB signals are clearer. In the time domain data in Fig.10F we see a very strong cratonic LAB separated by a sharp step from the western LAB. In Fig.10E the cratonic LAB is also clearly visible. In this 3° latitude wide profile we find also indications of the western dipping MLD which suggests strong heterogeneities here. Our observations of the cratonic LAB indicate, together with other S-receiver function observations (Miller and Eaton, 2010 in Canada and Kind et al., 2013 in Scandinavia), that the deep cratonic LAB is visible in converted waves. A study of the complete USArray data in the east is required for a more comprehensive analysis of the cratonic LAB. Close to the east coast the LAB again seems to occur near 100 km depth (Rychert et al., 2007).

4.5 View on the discontinuities with unfiltered S receiver functions (Fig.11)

In Fig.11 the same data are shown as in Fig.10, except that no filter is applied apart from the deconvolution. The data are much shorter period than in Fig.10. If a discontinuity is sharp we expect that its signal also gets sharper if a shorter period filter or no filter is applied. This seems not to be the case for all the upper mantle discontinuities observed in this study such as the western and cratonic LAB and MLD. The discontinuities seem to dissolve in a sequence of sharper discontinuities with a very scattered appearance with sometimes a relatively short correlation length. A kind of scattered lamella structure with stepwise decreasing velocity could cause such signals. This means that these discontinuities are in reality transition zones with stepwise decreasing velocities. A lamella structure of the upper mantle has been observed in long range controlled source profiles for a long time, for example in Phanerozoic western Europe (see Kind, 1974) and in the cratons of northern Eurasia (see Mechie et al., 1993) and North America (see Thybo and Perchuc, 1997). No phases are marked in Fig.11 in order not to bias the reader. Generally the same phases as in Fig.10 are also visible in Fig.11, however, as groups of scattered signals. The signal with the largest amplitudes is the western LAB, especially in Fig.11F. It spreads out over more than 5 sec which corresponds to at least 50 km. We see in Fig.11A the east dipping western LAB reaching far below the MLD. West dipping structures are visible in Figs.11C and especially clearly in Fig.11D. The connection between these structures and the cratonic MLD seems obvious. As in the north, indications of an east dipping structure are also observed in Fig.11E and Fig.8I. The sharp step between the western LAB und cratonic LAB near 105°W is also clear in the unfiltered data in

Fig.11F as in the longer period filtered data in Fig.10F.

How do our observations agree with earlier seismic images of the mantle lithosphere in the western and central US? Levander and Miller (2012) also used S-receiver function data from USArray in the same area. They also observe the break in the LAB along the Sevier Thrust Belt. However they interpret the deep velocity drop east of the Sevier Thrust Belt as the cratonic LAB of the Laurentia plate. They do not report on the MLD and a west-dipping structure between the Rocky Mountains front and the Sevier Thrust Belt. Hopper et al. (2014) observed in the Yellowstone region the same break in the mantle lithosphere, also using S-receiver functions. They observed east of Yellowstone a faint shallow MLD but no west-dipping structure. Hansen et al. (2013) observed the LAB below the Colorado Plateau at 100 to 150 km depth and east of it at 150 to 200 km depth. This agrees with our LAB observations along 38°N (Fig.8l). Foster et al. (2014) also studied the lithosphere in the American Midwest with USArray S-receiver functions. They observed east of about 98°W a strong MLD near 100 km depth and the cratonic LAB at 200-250 km depth. Their data are close to our profile shown in Fig.8d. We also see here a strong MLD east of about 98°W. However we see, in addition, indications of the east-dipping LAB and the west-dipping MLD within the 2° latitude wide profile in Fig.8d. Lekic and Fischer (2014) observed below the Colorado Plateau and surroundings scattered negative signals near 100 km depth in S-receiver functions which they interpreted as the LAB beneath the Basin and Range Province and the Rocky Mountains front, west and east of the Colorado Plateau, respectively. Beneath the stable Colorado Plateau and the Great Plains they interpreted a negative phase in the same depth range as the MLD. We observe below the Colorado Plateau the LAB of the **western** US at about 100 km depth (Fig.9c).

5. Anisotropy of the MLD?

Sodoudi et al. (2013) found in South Africa MLD signals in S receiver functions showing azimuthal anisotropy. They observed a sign change of the S-to-P converted signal from about 85 km depth with a periodicity of 180° backazimuth. The MLD in our data does not show any sign change or significant change of the amplitudes as a function of the backazimuth (see LVZ1 in Fig.5). This means that there are no indications in our data for azimuthal anisotropy as the cause of the MLD signal in the cratonic US. **The azimuthal coverage of seismic sources is good for the identification of azimuthal periodicities (see Fig.2). By far most sources are concentrated in opposing azimuths (Alaska and the Aleutians versus the Andes and the south-western Pacific versus the eastern Mediterranean). The missing anisotropy in MLD S-receiver function data (Fig.5) seems to be in**

contradiction to the anisotropy model obtained from a joint inversion of tomography and SKS data (Yuan and Romanowicz, 2010). **The reason for this discrepancy is still unknown.**

6. Low velocity zone above the 410-km discontinuity.

Tauzin et al. (2010) observed a nearly global velocity reduction at about 350 km depth without any relation to surface tectonics. The cause of this low velocity layer is thought to be partial melt caused by dehydration (Bercovici and Karato, 2003). We observed a similar discontinuity in the USArray S-receiver functions (see e.g. Figs.4 and 9). Jordan and Paulson (2013) suggested that a low viscosity zone directly above the 410 discontinuity decouples the thick cratonic tectosphere from the flowing mantle. Looking at Fig.9 it seems that the strongest signals of the phase LVZ410 are observed in the western US where the LAB occurs at about 100 km depth. The signal is weaker in the cratonic US (Fig.9b,c,g). This means that the velocities directly above the 410 are lower in Phanerozoic regions than in cratonic regions of the US. This supports the tomographic results summarized by Jordan and Paulson (2013) of the cratonic tectosphere **having higher velocities** down to the 410-km discontinuity.

7. Conclusions

We have been able to image with S-receiver functions the major seismic discontinuities in the upper mantle below large regions of the western and central United States. In the upper 200 km we see complicated structures of the western LAB and the MLD (Fig.12). The east-dipping LAB interferes with the west plunging MLD in a complicated manner. We interpret these structures as being caused by the continental collision of the Farallon plate and the Laurentia plate. The MLD appears to be deformed in this collision in a similar way as could be expected for a shallow non-cratonic LAB. This could mean that the Archean lithosphere of the craton (Yuan and Romanowicz, 2010) was deformed during the collision with the Farallon plate. The western LAB dips **partly** far to the east to the mid-continental rift system, where it could be mistaken for the cratonic LAB. The deep cratonic LAB near 200 km depth is weakly observed at the eastern end of the considered area (from about 90 to 82°W). Its connection to the previously observed shallow LAB near the Atlantic coast needs further investigation with all eastern USArray data. **The cratonic LAB is very strong in the south-western part of the US.** Below 200 km depth we have observed a scattered Lehmann discontinuity, which is considered to be the bottom of the asthenosphere. Directly above the 410 km discontinuity mainly in the western US we observed a strong velocity reduction. Such a velocity reduction directly above the 410 is not observed in the cratonic US, which indicates higher velocity here.

Acknowledgments

This research was supported by the Deutsche Forschungsgemeinschaft. The facilities of the IRIS Data Management System, and specifically the IRIS Data Management Center, were used for access to waveform and metadata required in this study (<http://ds.iris.edu/data/>). The IRIS DMS is funded through the National Science Foundation and specifically the GEO Directorate through the Instrumentation and Facilities Program of the National Science Foundation under Cooperative Agreement EAR-1063471. We also wish to thank Gene Humphreys and Shun Karato for discussions, and Theresia Ziegs and Irene Kind for help in the data processing.

References

- Abt, D. L., K.M. Fischer, S.W. French, H.A. Ford, H. Yuan and B. Romanowicz (2010), North American lithospheric discontinuity structure imaged by Ps and Sp receiver functions, *J. Geophys. Res.*, *115*, B09301, doi:10.1029/2009JB006914.
- Barrell, J. (1914), The strength of the Earth's crust, *J. Geology*, *22*, 655–683.
- Bercovici, D. and S. Karato (2003) Whole mantle convection and transition-zone water filter. *Nature* *425*, 3944.
- Bock, G. (1994), Multiples as precursors to S, SKS and ScS. *Geophysical Journal International* *119*, *2*, 421-427.
- Bodin, Th., H. Yuan and B. Romanowicz (2014) Inversion of receiver functions without deconvolution-application to the Indian craton. *Geophysical Journal International* *196*, *2*, 1025-1033, doi:10.1093/gji/ggt431.
- Bunge, H.-P. and S.P. Grand (2000), Mesozoic plate-motion history beneath the northeast Pacific ocean from seismic images of the subducted Farallon slab. *Nature* *405*, 337-340.
- Eaton, D.W., F. Darbyshire, R.L. Evans, H. Grütter, A.G. Jones and X. Yuan (2009), The elusive lithosphere–asthenosphere boundary (LAB) beneath cratons. *Lithos* *109*, 1-22, doi: 10.1016/j.lithos.2008.05.009.

- Foster, K., K. Dueker, B. Schmandt and H. Yuan (2014), A sharp cratonic lithosphere–asthenosphere boundary beneath the American Midwest and its relation to mantle flow. *Earth and Planetary Science Letters* 402, 82-89.
- Fischer, K.M., H.A. Ford, D.L. Abt and C.A. Rychert (2010) , The lithosphere–asthenosphere boundary. *Annual Review of Earth and Planetary Sciences* 38, 551–575. doi:10.1146/annurev-earth-040809-152438.
- Fuchs, K. and G. Müller (1971) Computation of synthetic seismograms with the reflectivity method and comparison with observations. *Geophys. J. Int.* 23 (4), 417-433, doi: 10.1111/j.1365-246X.1971.tb01834.x
- Grand, S. (1994), Mantle shear structure beneath the Americas and surrounding oceans, *J. Geophys. Res.*, 99, 11,591–11,621.
- Gu, J.Y., A.M. Dziewonski and G. Ekström (2001) Preferential detection of the Lehmann discontinuity beneath continents, *Geophys. Res. Lett.* 28, 4, 4655-4658.
- Hansen, S., K. Dueker, J. Stachnik, R. Aster and K.A. Karlstrom (2013), A rootless rockies—Support and lithospheric structure of the Colorado Rocky Mountains inferred from CREST and TA seismic data, *Geochem. Geophys. Geosyst.* 14 (8), 2670–2695, <http://dx.doi.org/10.1002/ggge.20143>.
- Hopper, E., H.E. Ford, K.M. Fischer and V. Lekic (2014), The lithosphere-asthenosphere boundary and the tectonic-magmatic history of the northwestern United States, *Earth Planet Sci. Lett.* 402, 69-81.
- Jones, C. H. and R. A. Phinney (1998), Seismic structure of the lithosphere from teleseismic converted arrivals observed at small arrays in the southern Sierra Nevada and vicinity, California, *J. Geophys. Res.*, **103**(B5), 10,065–10,090, doi:10.1029/97JB03540.
- Jordan, T. H. (1975), The continental tectosphere, *Rev. Geophys. Space Phys.*, 13, 1–12.
- Jordan, T. H., and E. M. Paulson (2013), Convergence depths of tectonic regions from an ensemble

of global tomographic models, *J. Geophys. Res. Solid Earth*, 118, 4196–4225, doi:10.1002/jgrb.50263.

Karato, S. (2012), The origin of the asthenosphere. *Earth and Planetary Science Letters* 321-322, 95–103, doi:10.1016/j.epsl.2012.01.001.

Kind, R. (1985) The reflectivity method for different source and receiver structures, *J. Geophys.*, 58, 146–152.

Kind, R., X. Yuan and P. Kumar (2012), Seismic receiver functions and the lithosphere-asthenosphere boundary. *Tectonophysics* 536-537, 25-43, doi:10.1016/j.tecto.2012.03.005

Kind, R., F. Sodoudi, X. Yuan, H. Shomali, R. Roberts, D. Gee, T. Eken, M. Bianchi, F. Tilmann, N. Balling, B.H. Jacobsen, P. Kumar and H.W. Geissler (2013), Scandinavia: A former Tibet? *Geochem. Geophys. Geosyst* 14, 4479–4487, doi:10.1002/ggge.2025.

Kosarev, G., R. Kind, S. V. Sobolev, X. Yuan, W. Hanka and S. Oreshin (1999), Seismic evidence for detached Indian lithospheric mantle beneath central Tibet, *Science*, **283**, 1306–1308.

Kumar, P., R. Kind and X.H. Yuan (2010), Receiver function summation without deconvolution. *Geophysical Journal International* 180, 3, 1223-1230, DOI:10.1111/j.1365-246X.2009.04469.x.

Kumar, P., X. Yuan, R. Kind, and J. Mechie (2012a), The lithosphere-asthenosphere boundary observed with USArray receiver functions. *Solid Earth* 3, 149-159, doi:10.5194/se-3-149.

Kumar, P., R. Kind, X. Yuan and J. Mechie (2012b), USArray receiver function images of the LAB, *Seismol. Res. Lett.*, 83, 486–491, doi:10.1785/gssrl.83.3.486.

Levander, A. and M.S. Miller (2012), Evolutionary aspects of lithosphere discontinuity structure in the western U.S., *Geochem. Geophys. Geosyst.*, 13, Q0AK07, doi:10.1029/2012GC004056.

Lekic, V. and B. Romanowicz (2011), Tectonic regionalization without a priori information: a cluster analysis of upper mantle tomography, *Earth Planet. Sci. Lett.*, 308, 151–160, doi:10.1016/j.epsl.2011.05.050.

Lekic, V. and K. Fischer (2014), Contrasting lithospheric signatures across the western United States revealed by Sp receiver functions. *Earth and Planet. Sci. Lett.*, 42, 90-98, <http://dx.doi.org/10.1016/j.epsl.2013.11.026>.

Li, X., X.H. Yuan and R. Kind (2007), The lithosphere–asthenosphere boundary beneath the western United States, *Geophysical Journal International*, 170 (2), 700–710 <http://dx.doi.org/10.1111/j.1365-246X.2007.03428.x>.

Kind, R. (1974), Long range propagation of seismic energy in the lower lithosphere, *J. Geophys.* 40, 189-202.

Mechie, J., A.V. Egorkin, K. Fuchs, T. Ryberg, L. Solodilov and F. Wenzel (1993) P-wave mantle velocity structure beneath northern Eurasia from long-range recordings along the profile Quartz. *Phys. Earth Planet. Inter.*, 79, 269-286.

Miller, M.S. and D.W. Eaton (2010), Formation of the cratonic mantle keels by accretion: Evidence from S receiver functions. *Geophys. Res. Letts.*, 37, L18305, doi:10.1029/2010GL044366.

Rychert, C., K. Fischer and S.A. Rondenay (2005), A sharp lithosphere–asthenosphere boundary imaged beneath eastern North America. *Nature* 436, 542–547, <http://dx.doi.org/10.1038/nature03904>.

Rychert, K., S. Rondenay and K. Fischer (2007), P-to-S and S-to-P imaging of a sharp lithosphere–asthenosphere boundary beneath eastern North America. *J. Geophys. Res.* 112, B08314, <http://dx.doi.org/10.1029/2006jb004619>.

Rychert, C.A. and P.M. Shearer (2009), A global view of the lithosphere-asthenosphere boundary. *Science* 324 (5926), 495–98.

Rychert, C.A., P.M. Shearer and K.M. Fischer (2010), Scattered wave imaging of the lithosphere–asthenosphere boundary. *Lithos.* 120, 173-185, doi:10.1016/j.lithos.2009.12.006.

Schaeffer, A. J., and M. G. Bostock (2010), A low- velocity zone atop the transition zone in northwestern Canada, *J. Geophys. Res.*, *115*, B06302, doi:10.1029/2009JB006856.

Schmandt, B. and E. Humphreys (2011), Seismically imaged relict slab from the 55 Ma Siletzia accretion to the northwest United States, *Geology* *39*, 175–178, doi: 10.1130/G31558.1.

Schmandt, B. and F.-C. Lin (2014), P and S wave tomography of the mantle beneath the United States, *Geophys. Res. Lett.*, *41*, 6342–6349, doi:10.1002/ 2014GL061231.

Selway, K., H. Ford and P. Kelemen (2015) The seismic mid-lithospheric discontinuity. *Earth and Planet. Sci. Lett.* *414*, 45-57, <http://dx.doi.org/10.1016/j.epsl.2014.12.029>.

Shearer, P.M. (1991), Constraints on upper mantle discontinuities from observations of long-period reflected and converted phases. *Journal of Geophysical Research-Solid Earth* *96*, B11, 18147-18182.

Sigloch, K., N. McQuarrie and G. Nolet (2008), Two-stage subduction history under North America inferred from multiple-frequency tomography. *Nature Geoscience*, *1*, 458–462, <http://dx.doi.org/10.1038/ngeo23.1>

Sigloch, K. (2011), Mantle provinces under North America from multifrequency P wave tomography. *Geochem. Geophys. Geosyst.* *12*, Q02W08, <http://dx.doi.org/10.1029/2010GC003421>.

Sodoudi, F., X. Yuan, R. Kind, S. Lebedev, J.M.-C. Adam, E. Kästle and F. Tilmann (2013), Seismic evidence for stratification in composition and anisotropic fabric within the thick lithosphere of Kalahari Craton, *Geochem. Geophys. Geosyst.*, *14*, 5393–5412, doi:10.1002/2013GC004955.

Tauzin, B., Debayle, E. and Wittlinger G. (2010), Seismic evidence for global low-velocity layer within the Earth's upper mantle. *Nature Geoscience* *3*, doi: 10.1038/NGEO969.

Thybo, H., Perchuc, E., 1997. The seismic 8 degrees discontinuity and partial melting in continental mantle. *Science* *275* (5306), 1626–1629.

Wilson, D.C., Angus, D.A., Ni, J.F., Grand, S.P. (2006), Constraints on the interpretation of S-to-P

receiver functions. *Geophys. J. Int.* 165, 969–980.

Yoshizawa, K. (2014), Radially anisotropic 3-D shear wave structure of the Australian lithosphere and asthenosphere from multi-mode surface waves. *Phys. Earth Planet. Inter.*, 235, 33–48, <http://dx.doi.org/10.1016/j.pepi.2014.07.008>.

Yuan, X., J. Ni, R. Kind, J. Mechie and E. Sandvol (1997), Lithospheric and upper mantle structure of southern Tibet from a seismological passive source experiment, *J. Geophys. Res.*, 102, 27,491–27,500.

Yuan, X., R. Kind, X. Li and R. Wang (2006), The S receiver functions; synthetics and data example. *Geophys. J. Int.* 165, 555–564 doi: 10.1111/j.1365-246X.2006.02885.x.

Yuan, H. and B. Romanowicz (2010), Lithospheric layering in the North American craton, *Nature* 466, 1063–1071, <http://dx.doi.org/10.1038/nature09332>.

Yuan, H. B. Romanowicz, K. Fischer and D. Abt (2011), 3-D shear wave radially and azimuthally anisotropic velocity model of the north American upper mantle, *Geophys. J. Int.*, 184, 1237–1260, doi:10.1111/j.1365-246X.2010.04901.x

Vinnik, L., Y. Ren, E. Stutzmann, V. Farra and S. Kiselev (2010), Observations of S410p and S350p phases at seismograph stations in California, *J. Geophys. Res.*, 115, B05303, doi:10.1029/2009JB006582.

Zheng Z. and B. Romanowicz (2012), Do double “SS precursors” mean double discontinuities? *Geophys. J. Int.*, 191, 1361–1373.

Figure captions

Figure 1: Map of North America with seismic stations (triangles) from USArray (<http://www.usarray.org/researchers/obs/transportable>), the Berkeley seismic network (<https://seismo.berkeley.edu>), the Southern California network (<http://www.scsn.org>), and the

permanent network of the US Geological Survey (<http://earthquake.usgs.gov/monitoring/ans/>). The data have been obtained from the IRIS data archive (<http://ds.iris.edu/data/>). Seismicity (blue crosses) and relevant geological units are marked (RMF-Rocky Mountains Front, SRP-Snake River Plain, YS-Yellowstone, ST-Sevier Thrust Belt, CP-Colorado Plateau, MCRS-Mid-Continental Rift System).

Figure 2: Epicenters of 1102 earthquakes used in our study. Black triangle marks the center of the network used. Black circles with labels indicate epicentral distances from the center. **Not all earthquakes have been recorded at all sites since the USArray stations were moved every two years.**

Figure 3: a) Display of binned S-receiver functions as a function of the epicentral distance. Each bin contains more than one thousand traces. Precursors of the S phase from S-to-P conversions in the upper mantle are marked with dashed black lines (410-conversion at the 410, LVZ410-conversion at a velocity reduction directly above the 410, Lehmann-Lehmann discontinuity, LVZ1, LVZ2- conversions at velocity reductions between Moho and Lehmann, Moho-conversion at the Moho). LVZ2 and Lehmann are more clear in Fig.4, they are marked here for comparison. Additional theoretical traveltimes curves of ScS, SKS, S-to-P conversions of ScS and SKS at the 410 and 660 discontinuities and at a possible discontinuity at 580 km depth (ScS410p, ScS580p, ScS660p, SKS410p, SKS580p, SKS660p), crustal multiples (SPmp) and SPn are marked in green. **b)** Ray paths of Sp, SPmp and SPn.

Figure 4: Display of binned S-receiver function traces along a **a)** west-east and **b)** south-north line. LVZ1 is the LAB in the western US and the MLD in the central US. Details of LVZ1 and LVZ2 are shown in the narrower profiles in Figs.8 and 9. “Lehmann” indicates the bottom of the asthenosphere, and LVZ410 marks a velocity drop above the 410 km discontinuity. Note that this discontinuity is only weakly observed at the eastern end of the line. “410” is the discontinuity at 410 km depth. Although these discontinuities are greatly averaged in this display, they appear very clearly.

Figure 5: Display of binned S-receiver functions as a function of the backazimuth (see Fig.2) of the source of each record, independent of epicentral distance. Only stations on the cratonic part of the US (east of 110°W) are used. The same phases as in Fig.4 are marked. Most phases do not show any clear dependence on the backazimuth. The only exception might be the 410 discontinuity, which is strongest for sources in the northwest quadrant.

Figure 6: Theoretical seismograms (vertical component) computed with the reflectivity method for comparison with the observed data in Fig.3a. The strong SPn phase after S agrees well with the data in Fig.3a. A disagreement between computed and observed seismograms is the source-side Pn in front of the S signal (this figure) which is not in the data (Fig.3a). This is a phase traveling as P along the surface on the source side and is continuously radiating S waves downward. At the receiver side these phases are converted back to P and travel again horizontally along the uppermost mantle and are observed on the vertical component. These phases are not observed in the real data probably because of heterogeneities in the real Earth.

Figure 7: Theoretical seismograms for different structures at the source and receiver sides. **a)** Moho is at 50 km depth at the source side, **b)** no crust at the source side. Moho depth is 40 km at the receiver side in both cases. The source crust causes a negative precursor before the receiver side S-to-P conversion at the Moho (see PmSmp ray path in **c)**), which could be mistaken as an indication of a velocity drop in the mantle below the Moho. Such phases will only be a problem in interpretations of single data traces. In receiver function processing of real data this should not be a problem since source side models and source depths are different for each record and these effects are erased by summation. **c)** ray paths of Smp and PmSmp.

Figure 8a-p: Depth migrated west-east S-receiver function profiles (see location map at the top of the figure). The width of each profile is 2° latitude with 1° overlap. The latitude of the profiles is marked at each profile. **The magenta dashed line is interpreted as the LAB of the Farallon plate, the yellow dashed line as the MLD and the green dashed line as the LAB of the Laurentia plate, respectively. The dashed black line is a low velocity zone above the 410 discontinuity. See text for a discussion of these discontinuities.**

Figure 9a-g: The same data and same correlation marks as in Fig.8 but summed along broader south-north and west-east profiles. The profile width and orientation is shown in the location maps at the top of the figure. Region **a)** (northernmost west-east profile) does not have any stations in Canada. However, due to the shallow incidence angle of the S-receiver functions, the mantle below southern Canada is also sampled by events from the northwest. The westernmost south-north profile **d)** shows only the western LAB in the mantle lithosphere. In profile **e)** we see at the southern and northern ends the western LAB, and in the central part the deep MLD. In profile **f)** we see the cratonic MLD (yellow), the cratonic LAB (green) and in the north the deep western LAB

(magenta). In the easternmost south-north profile **g**) we see the MLD and weakly the cratonic LAB. See Fig.1 for explanation of the abbreviations of tectonic units.

Figure 10: West-east S-receiver function profiles in the time domain. The latitude of the distribution of piercing points in 200 km depth is marked in each panel. The data are filtered with an eight seconds low-pass filter. Correlated phases are marked with the same colors as in Figs.8 and 9, except that here black represents the LAB of the Juan de Fuca plate.

Figure 11: The same profiles as in Fig.10 but with no filter applied.

Figure 12: Visualization of the interfingering of the colliding Farallon LAB in the west with the Laurentia MLD in the east. The cratonic LAB is left out of the figure. The profiles in Figs.9a,b,c and Figs.10A, D and F represent the east dipping part of the Farallon LAB in the north, the west dipping Laurentia MLD and the flat part of the far east reaching Farallon plate in the south. The lateral transition between these three parts is in reality not as sharp as indicated here, but much more heterogeneous.

FIGURES

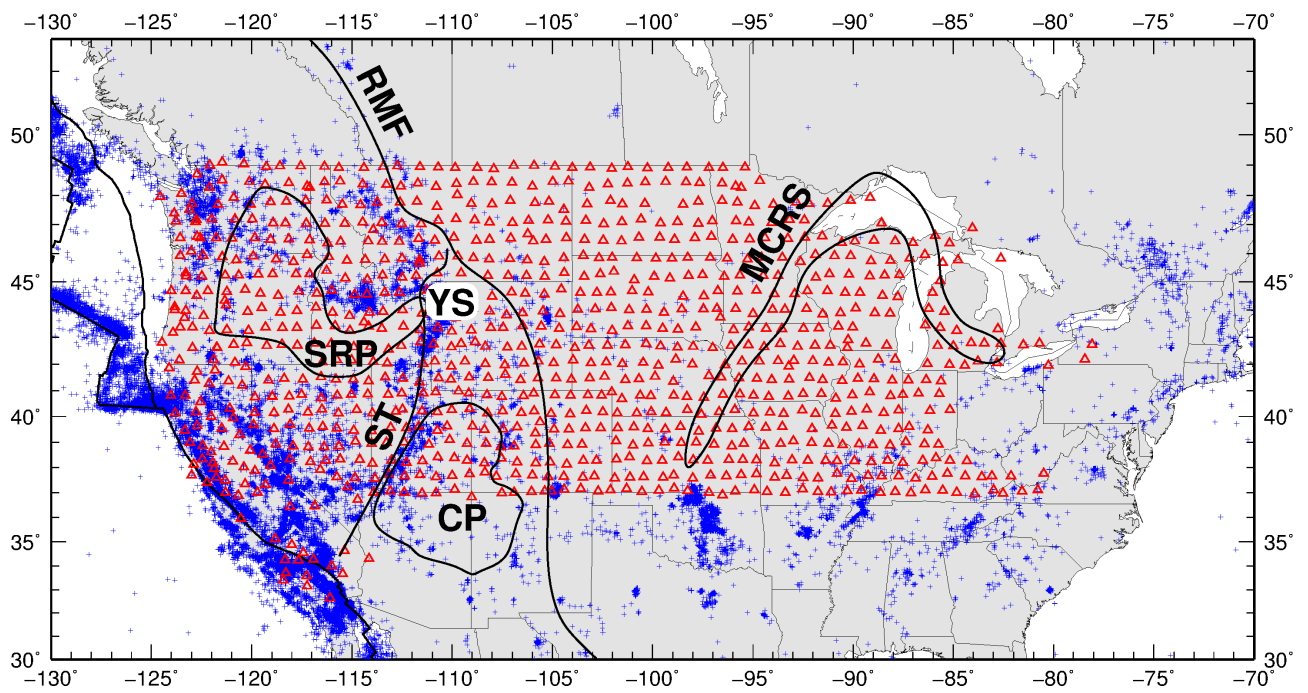


Figure 1

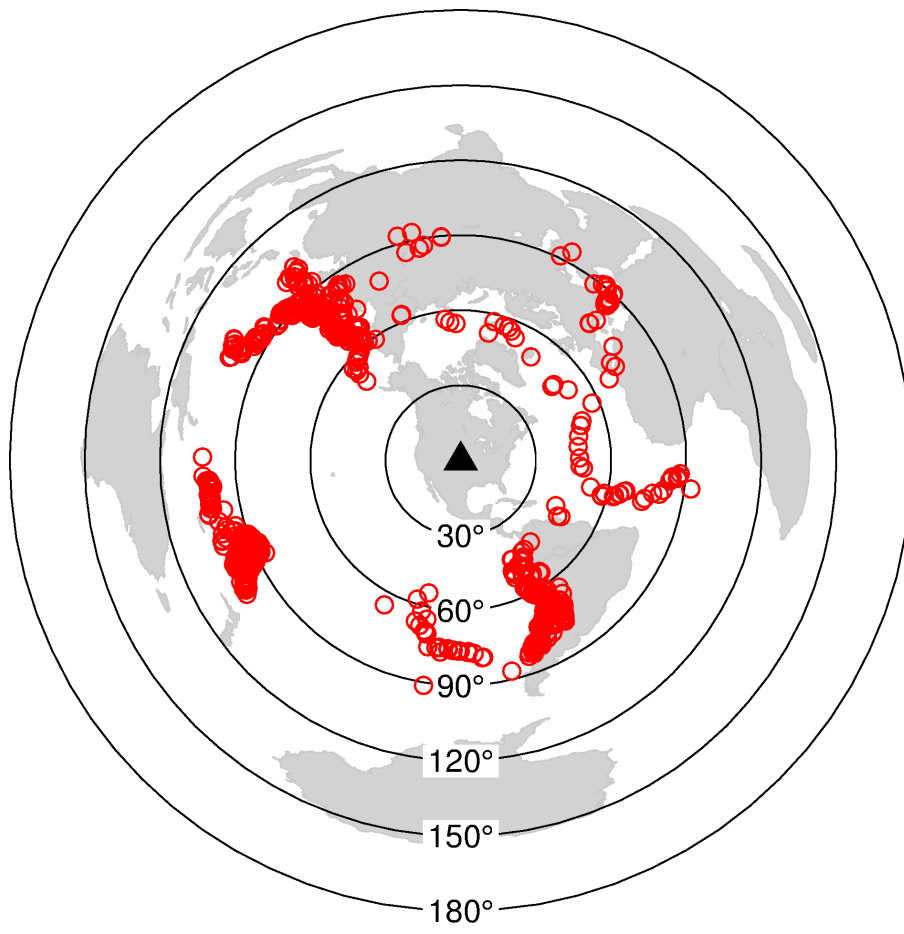


Figure 2

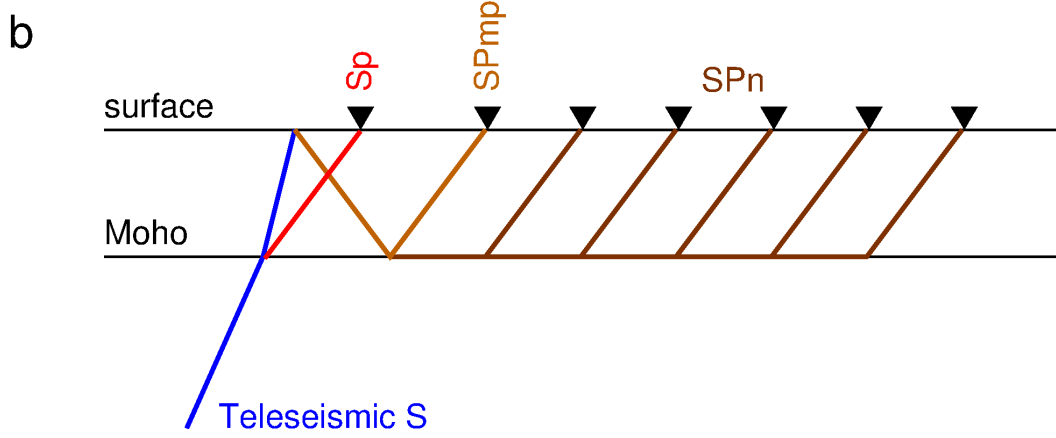
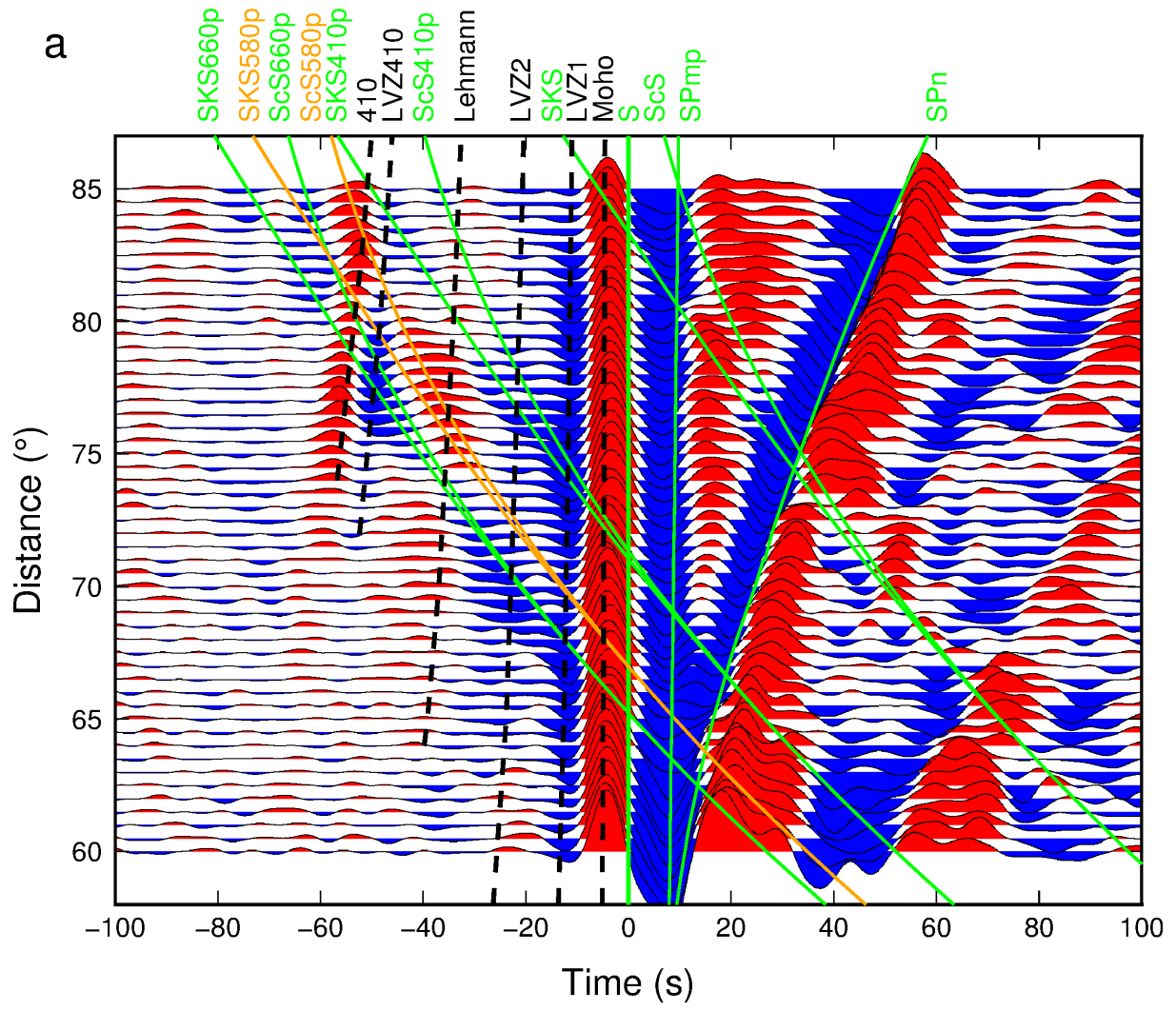


Figure 3

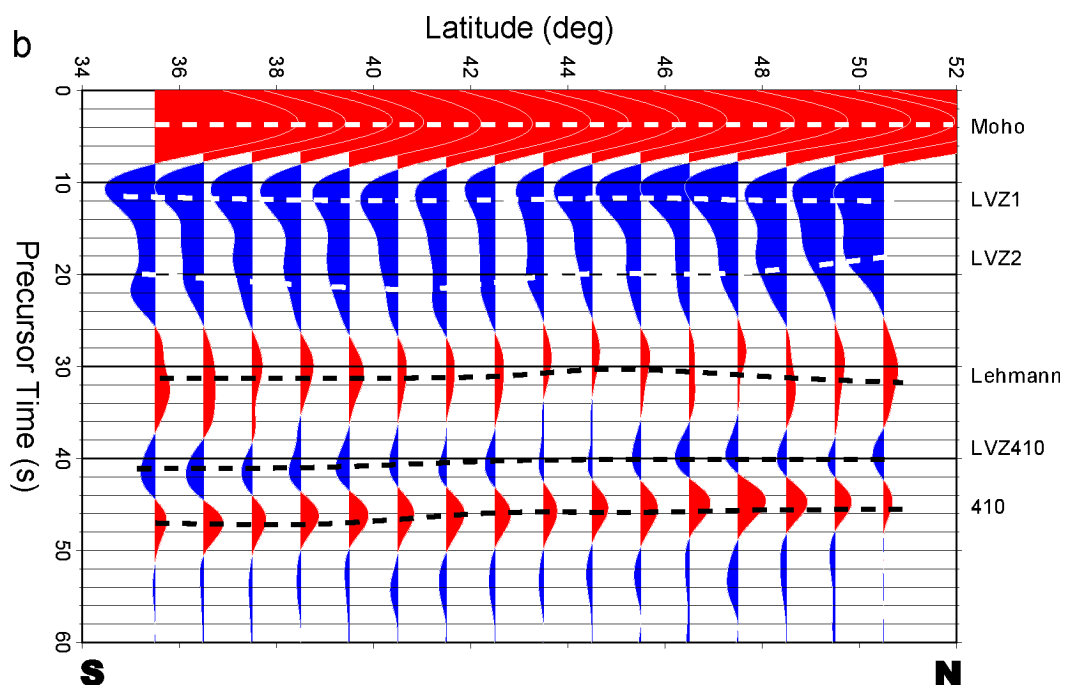
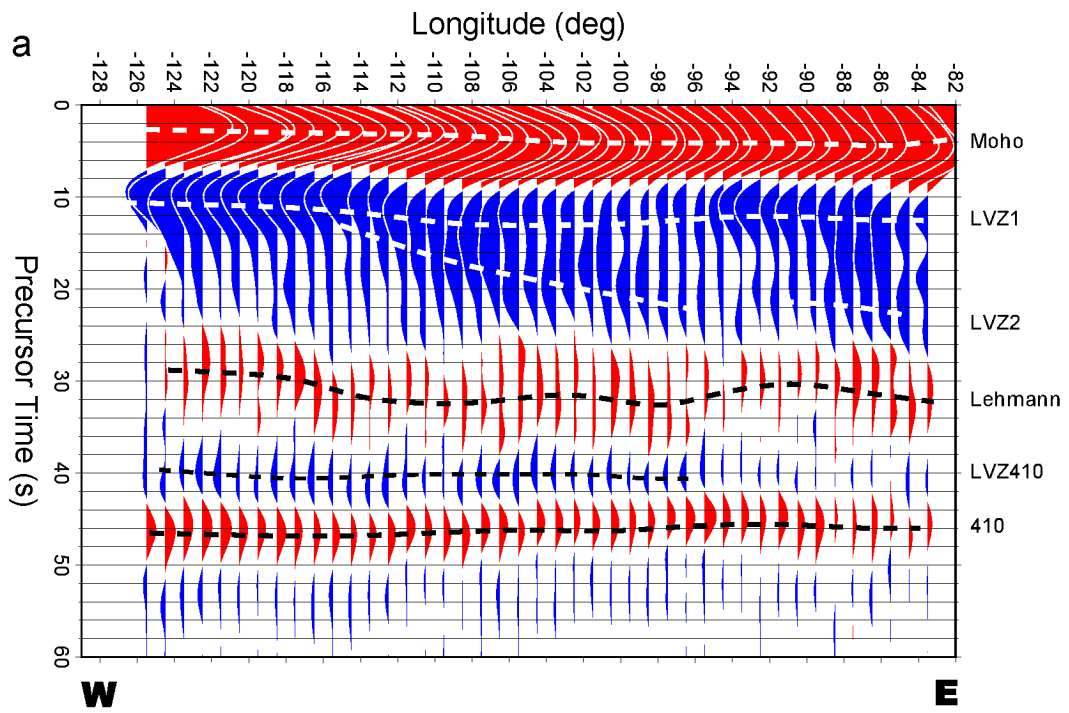


Figure 4

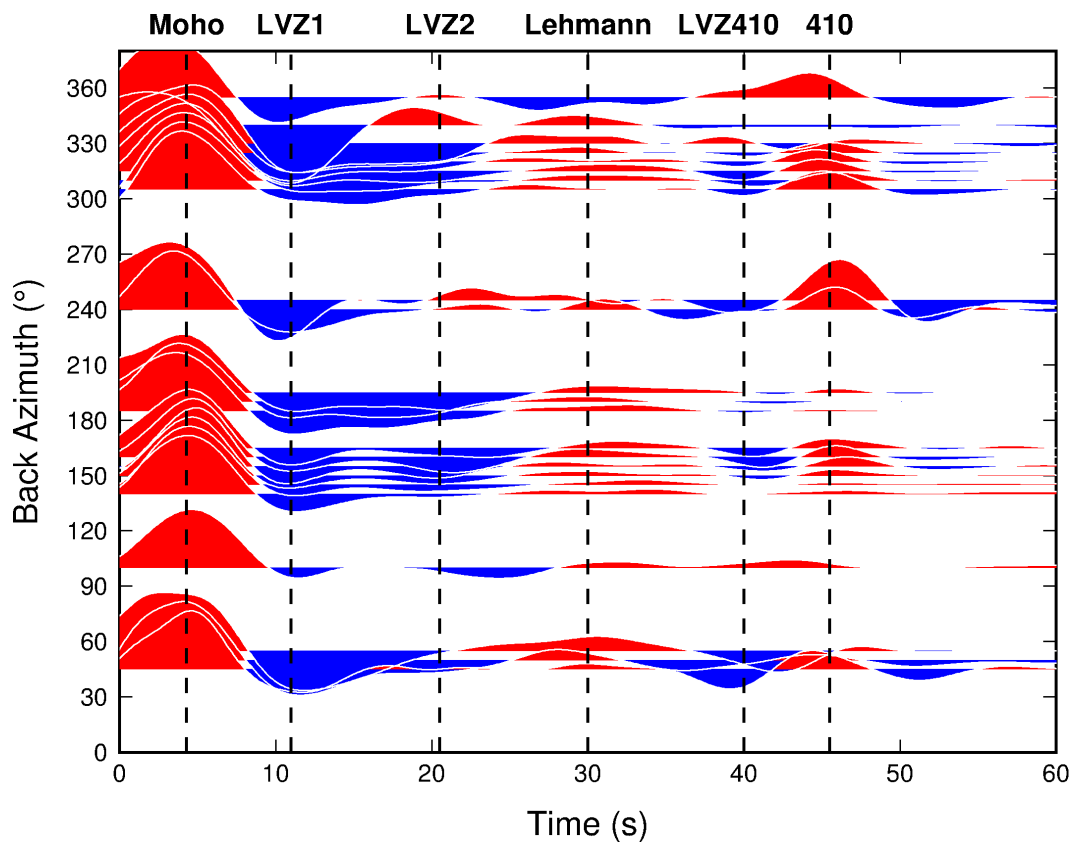


Figure 5

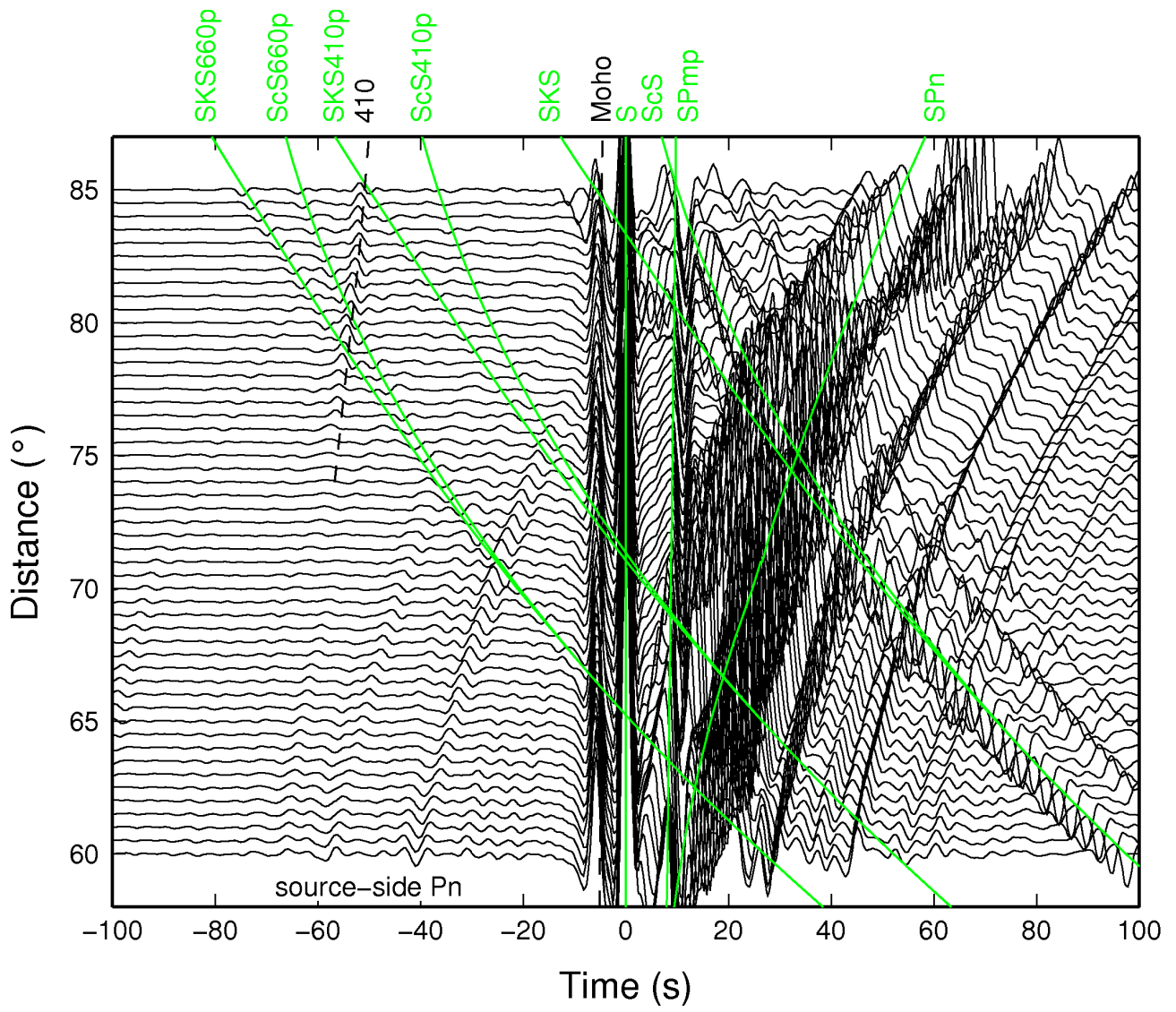


Figure 6

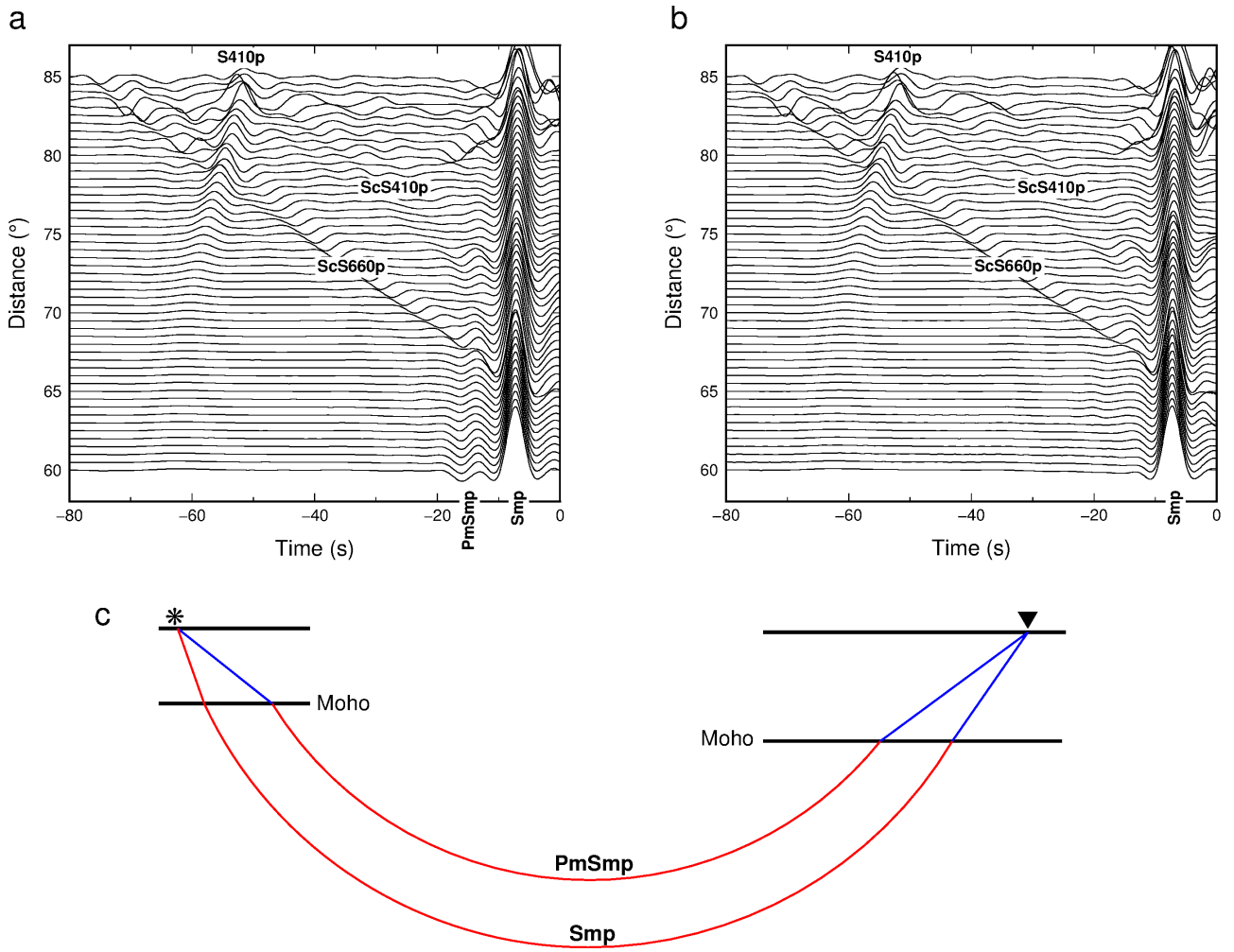


Figure 7

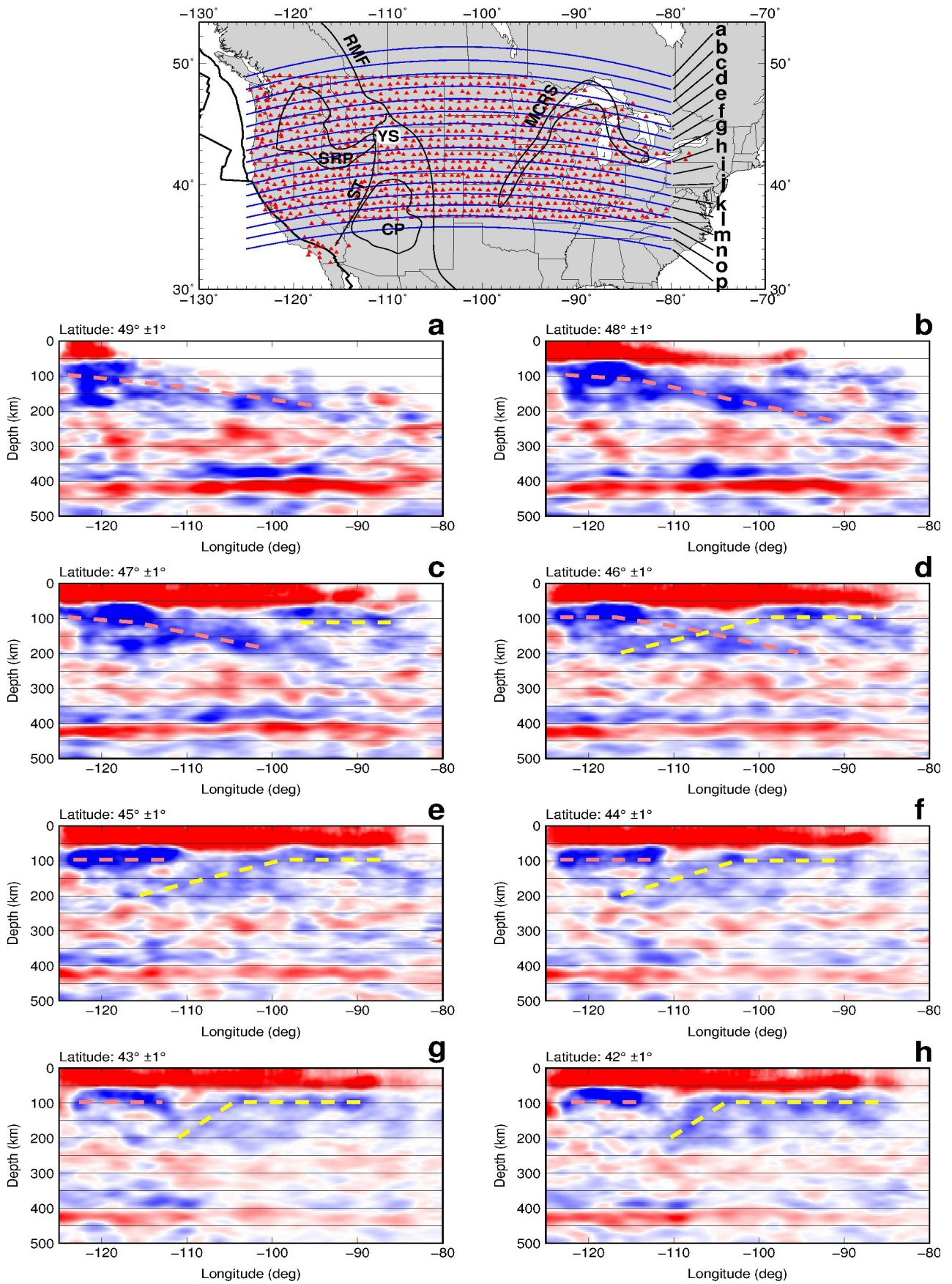


Figure 8a-h

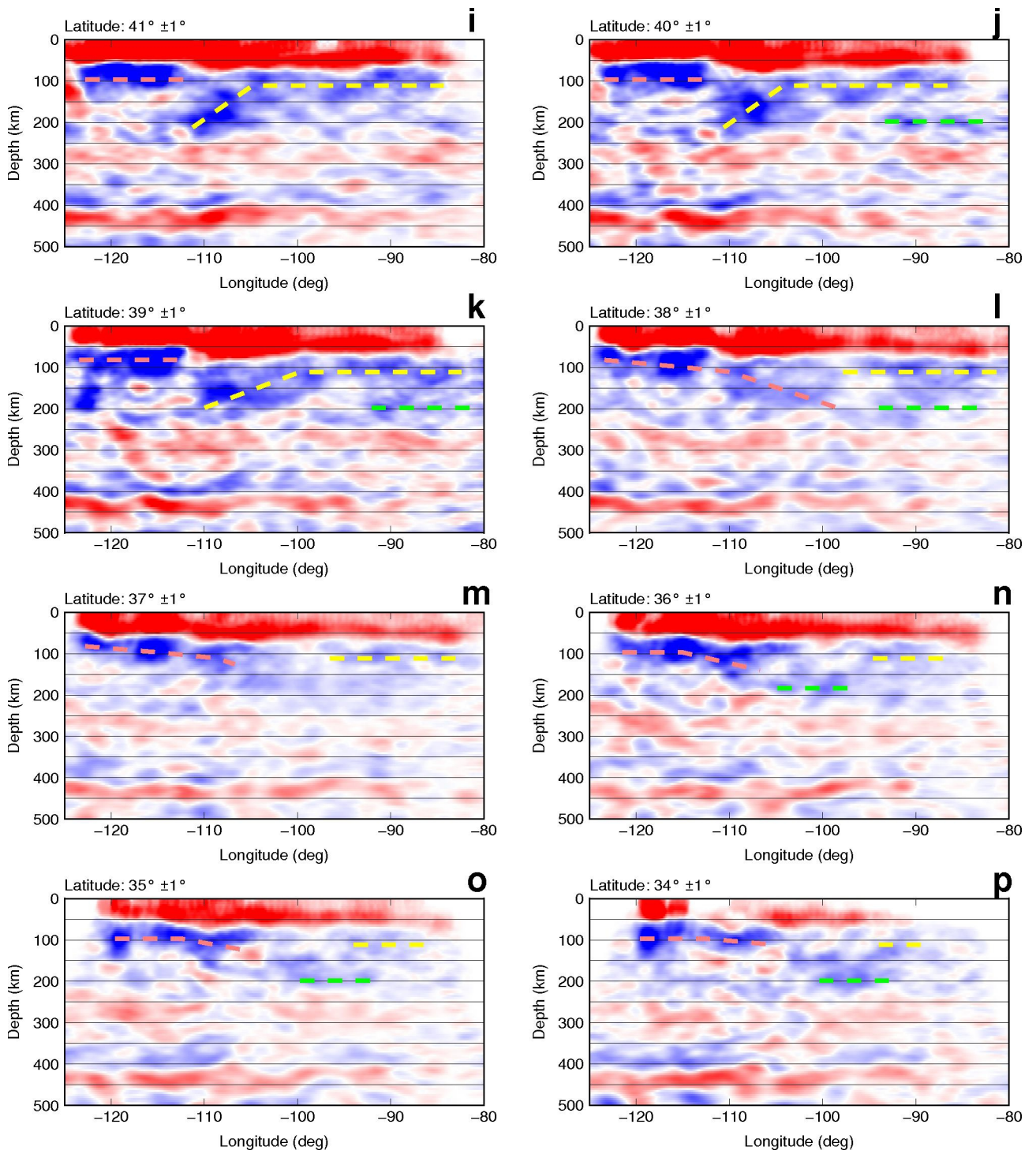


Figure 8i-p

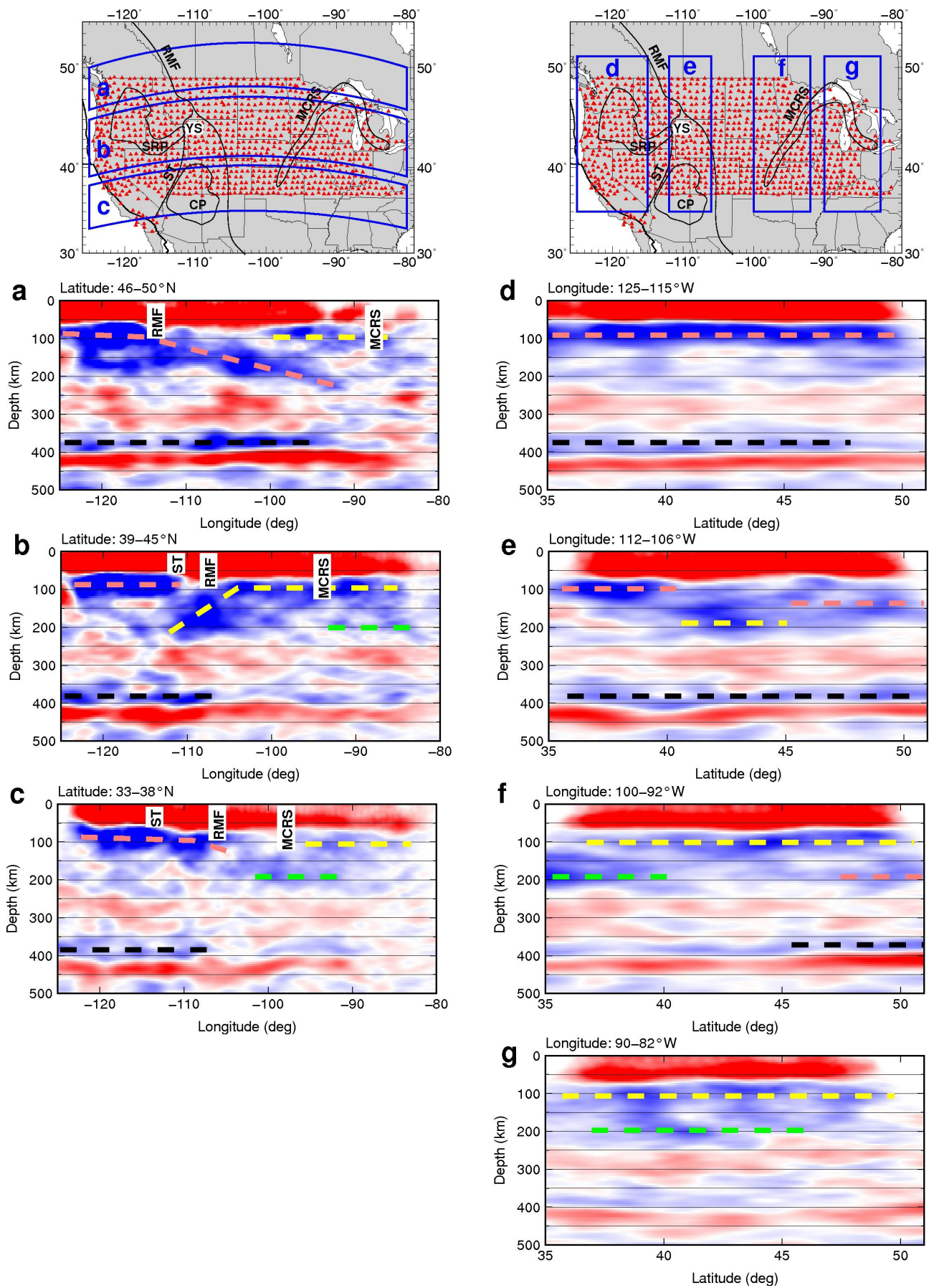


Figure 9

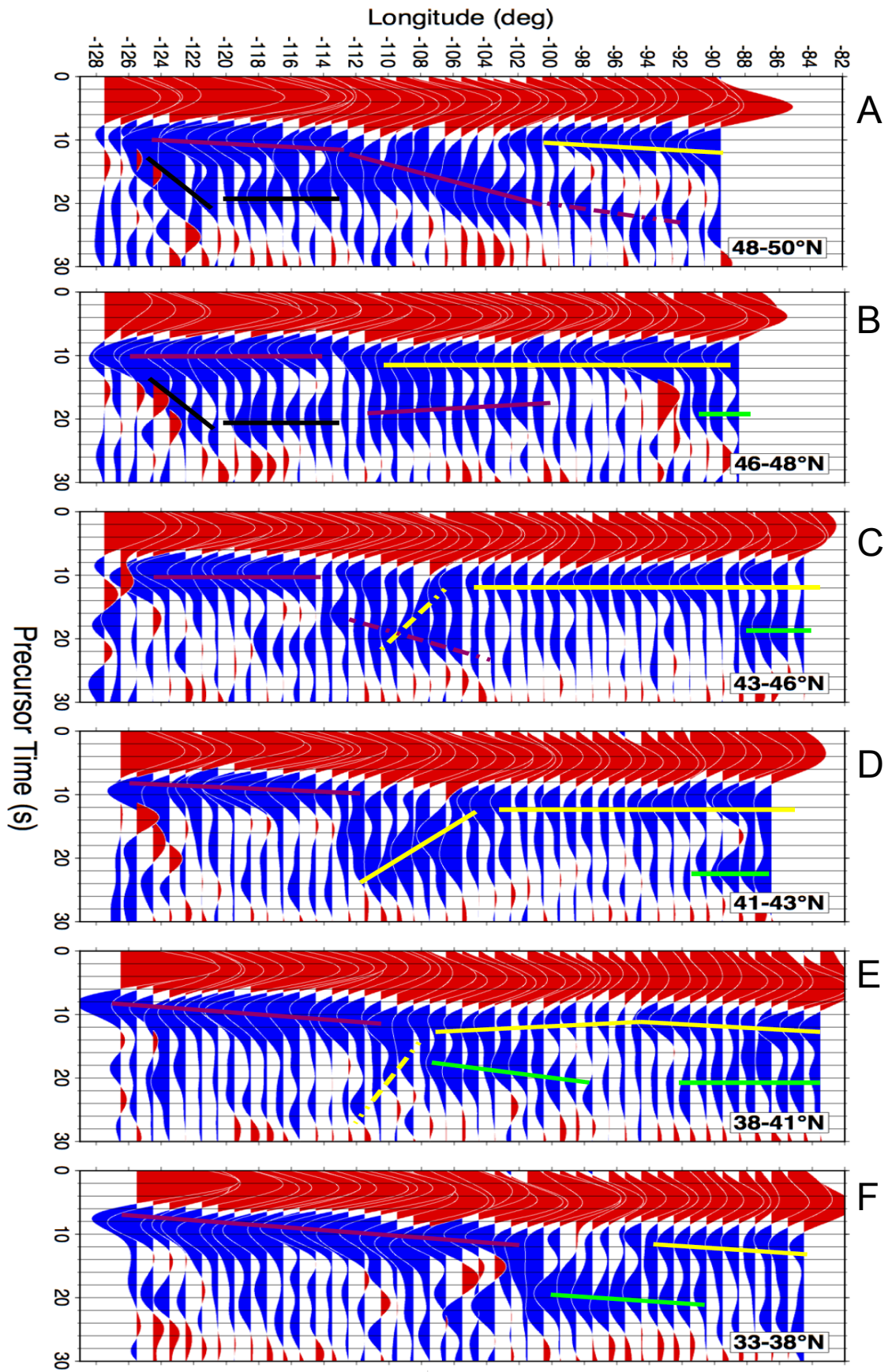


Figure 10

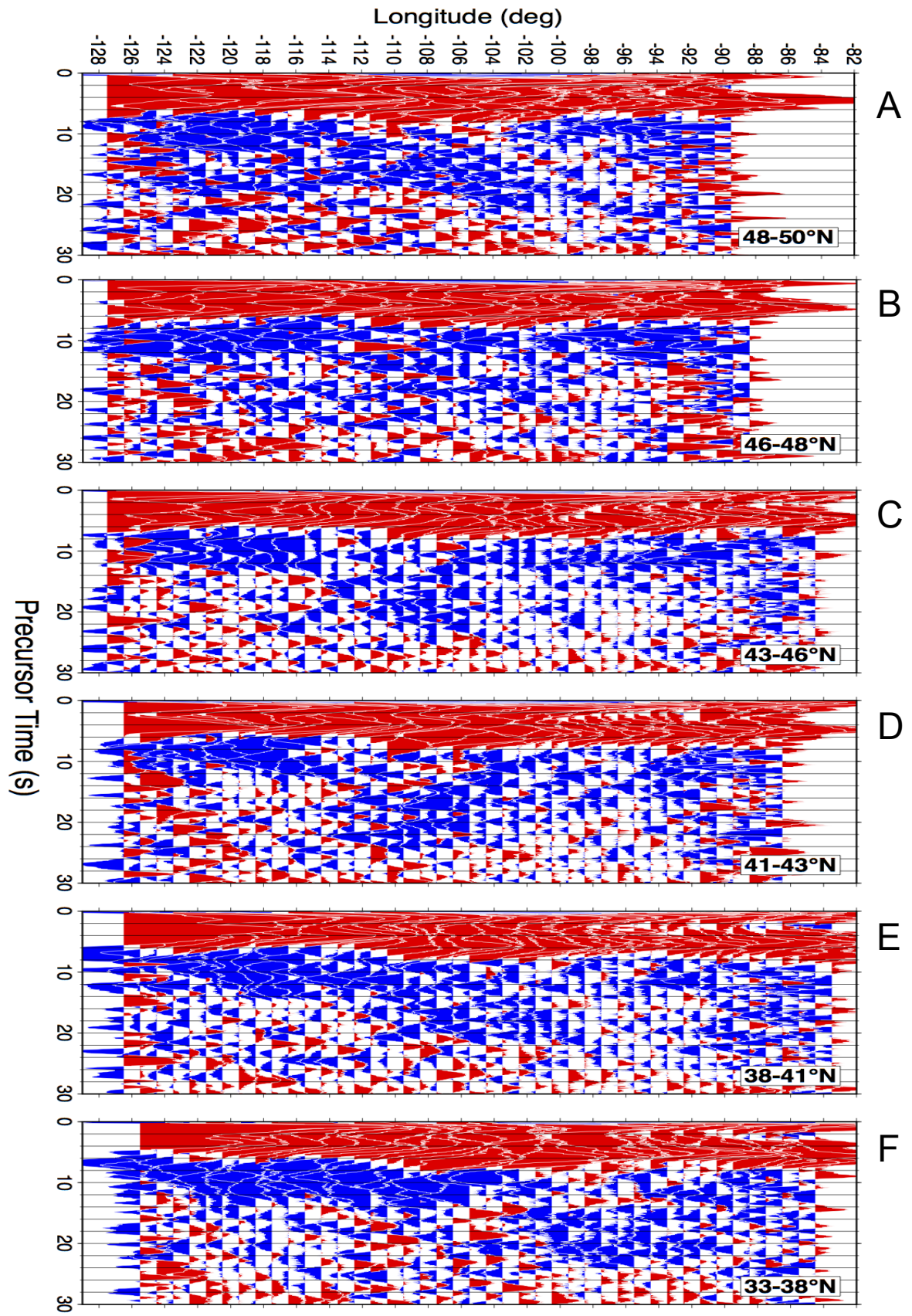


Figure 11

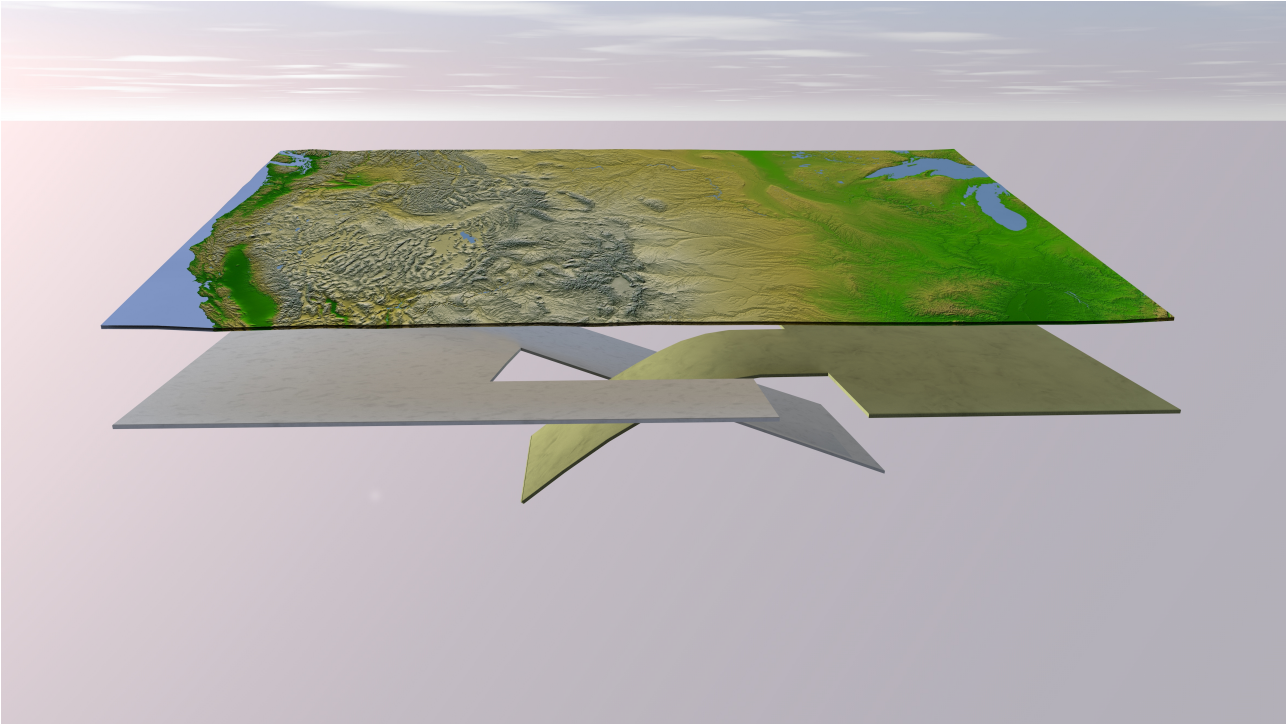


Figure 12